كلية الهندسة بشبرا
FACULTY OF ENGINEERING AT SHOUBRA
ERJ
PRINT ISSN 3009-6049
ONLINE ISSN 3009-6022

ENGINEERING RESEARCH JOURNAL (ERJ)
Volume (53) Issue (4)
October. 2024, pp:81-88
https://erjsh.journals.ekb.eg

Accuracy Assessment of UAV Photogrammetric Mapping

Maha F. Refaei[1]*, Mohamed Zaharan[1], Mahmoud S. Gomaa[1], Ayman M.Bayomy[1]

[1] Department of Surveying Engineering, Faculty of Engineering at Shoubra, Benha University, Cairo, Egypt.
* Corresponding Author.
E-mail: mohamedmedhat1991@gmail.com , Mohamed.zahran01@feng.bu.edu.eg, Mohamed.goma@feng.bu.edu.eg, ayman.soliman@feng.bu.edu.eg

Abstract: Due to technological developments, unmanned aerial vehicles (UAVs) have become a valuable tool in numerous applications including 3D spatial information extraction. UAV imagery can be employed efficiently to generate dense point clouds, digital surface models and orthoimages in short period of time. The aim of this research is to assess the accuracy of point clouds and orthoimages resulted from UAV photogrammetric mapping. A block of 70 UAV images captured with 80 % overlap and 80 % side lap at altitude of nearly 174m above ground is used. Many variables influencing the accuracy have been tested and evaluated which include percentage of overlap, georeferencing technique, configuration of ground control points, image resolution, as well as matching variables. The results showed that higher values of image overlap and image resolution improved positioning accuracy of the generated point cloud. Good accuracy results are yielded by using direct and indirect georeferencing techniques. Also, the limits of key/tie points have a significant impact on positioning accuracy and processing time. The positioning accuracy of a few centimeters was achieved for the generated point cloud. It was found also that generated orthomosic has high accuracy with RMSE values of 0.009m and 0.017m in the east and north directions, respectively, by using indirect georeferencing. The equivalent RMSE values were 0.020m and 0.019m considering direct georeferencing.

Keywords **:** UAV Imagery, SfM, Agisoft Photo Scan, Digital Image Processing

1. INTRODUCTION

UAV photogrammetry comprises the use of an aerial photogrammetric survey platform that can be remotely operated, semi- or fully-autonomously. In general platform carries: 1) a multispectral or infrared digital camera system to capture images; 2) a Global Navigation satellite System (GNSS) receiver to provide position for each frame; 3) an Inertial Measurement Unit (IMU) composed by gyroscopes, accelerometers, barometers and compass, which allows determination of the exterior orientation for each image taken during the flight; 4) a small CPU that controls all systems; and 5) a radio link that enables data download and human control by a remote system [1]. Processing software developed for UAV imagery have a much larger degree of automation compared with the classical photogrammetry software. Only, the images and the coordinates of each frame are required. Camera calibration parameters and external orientation angles are optional because they can be determined implicitly by the software [2]. Having camera positions from onboard GNSS, photogrammetric processing can be accomplished automatically. However, it is necessary to use ground control points and check points for quality control [3].

The growth and development of UAV as a photogrammetric platform, along with the advances in computer vision and image processing algorithms have resulted in using UAV Photogrammetry in several topographic applications [4]. Computer vision software algorithms rely on extracting, describing, and matching tie points from the overlapping images to generate 3D point clouds. Gerke [5] compared image acquisition by UAV versus conventional platforms, and presented the advances within photogrammetry and computer vision. The positioning accuracy obtained from images captured by micro-UAVs depends on several factors, including flight design, camera quality, camera calibration, processing algorithms and georeferencing approach [6].

Pessoa et al. [7] investigated the positional error of digital surface models generated using the post-processing of data acquired with a SenseFly eBee Classic, considering different configurations of ground control points (GCPs). A single

flight was conducted over a test field located at an urban region. RMSE values of about 3 times the ground sample distance (GSD) in horizontal direction and 5 times GSD in vertical direction are achieved using at least three well-distributed GCPs. Agüera-Vega et al. [8] explores the influence of flight altitude, terrain morphology, and the number of GCPs on DSM and orthoimage accuracies obtained with UAV photogrammetry. The results showed that the number of GCPs affected the accuracy in horizontal and vertical directions, whereas terrain morphology had no impact. In addition, the vertical accuracy was influenced by flight altitude. The accuracy decreased as flight altitude increased. Elkhrachy [9] obtained accurate geospatial 3D data from UAV images. Four different GCP distributions were tested using two different processing software packages; Agisoft Metashape and Pix4dmapper. The best horizontal RMSE values obtained ranged from 4cm to 6cm whereas the best vertical RMSE values achieved ranged from 5cm to 6cm.

Domingo et al. [10] assessed the influence of image resolution, camera type and side overlap on prediction accuracy of biomass models constructed from ground-based data and UAS data. The results showed that images captured with RGB camera using fine resolution led to better accuracy. The authors proposed forward overlap of 90% and side overlap of 70% to reduce the flight time and thus the cost of acquisition.

This research aims at: 1) determination of accurate 3-D positions, and generation of high-resolution orthoimage utilizing UAV imagery using different setups; and 2) accuracy assessment of obtained 3-D positions and generated orthoimages, through investigating the impact of many variables on the positioning accuracy.

The rest of the paper is presented in the following sections. Section 2 describes the study area and presents the used datasets. Section 3 introduces the processing methodology. Section 4 explains the photogrammetric data processing. Section 5 discusses the results. Section 6 concludes the results.

2.STUDY AREA AND USED DATASET

The test area is located in Switzerland centered nearly at latitude of 46º 3' 7.63" N and longitude of 6º 40' 55.16" E (defined in WGS84). Figure 1 shows the test area on Google earth with the red rectangle exhibiting the extent of the planned flight area. The area contains many different terrain features such as roads, buildings and vegetation.

FIG 1. Test area

Regarding the photogrammetric test, seventy UAV images with nearly 80% overlap and 80% side lap were captured. 18 ground reference points, distributed within the test area, were selected and determined in WGS84 using static GNSS with post processing technique resulting in an accuracy of 5mm. Figure 2 shows the distribution of the ground reference points.

On the other hand, the camera perspective center coordinates for each image were determined in WGS84 using GNSS real time kinematic technique. The imagery has been acquired using a 5 mm focal length Canon DIGITAL IXUS 120 IS camera at a flying height of about 174 m above ground. The image format is 4000 pixel by 3000 pixel, with image pixel size of 1.55µm by 1.55µm. Fig. 3 is a typical example of the obtained images.

FIG2. The distribution of the ground reference points

FIG 3. A typical example of the UAV aerial imagery

3.PROCESSING APPROACH; STRCTURE FROM MOTION

Structure-from-Motion (SfM) approach is adopted in this research to process captured UAV imagery. This approach operates according to the same basic principles as stereo photogrammetry. 3D structure of the scene can be resolved from a series of overlapping offset images. However, it differs fundamentally from conventional photogrammetry in that the geometry of the scene, camera positions and orientation are solved automatically without the need to specify a network of targets with known 3D positions. The solution adopts a highly redundant bundle adjustment procedure based on automatically extracted features from a set of multiple overlapping images [11].

Developed in the 1990s, SfM has its origins in the computer vision community [12, 13]. It evolved by the development of automatic feature-matching algorithms [14]. To determine the 3-D location of points within a scene, traditional digital photogrammetric methods require the 3-D position and orientation of the cameras, or the 3-D location of a set of control points to be known. Contrarily, the SfM approach requires no such data prior to scene reconstruction. It uses automatically matched features in multiple images for camera orientation and scene reconstruction. These features are tracked from image to image enabling initial estimates of camera positions and object coordinates which are then refined iteratively using least-squares minimization, as multiple solutions become available from the wide range of matched features [11]. Thus, the 3-D point clouds are generated in image-space which can be aligned to object-space coordinate system through scaling and orientation. In most cases, the transformation can be attained using a 3-D similarity transform based on a small number of ground control points with known object-space coordinates [15].

4.PHOTOGRAMMETRIC DATA PROCESSING

After accomplishment of the photogrammetric mission, the obtained UAV imagery were processed using the image processing software Agisoft Photo Scan, one of the popular software packages adopting SfM approach. Image processing by the SfM procedure is divided into two main steps [16]. The first step is image matching by the Scale-Invariant Feature Transform (SIFT) algorithm in which acquired images are employed as input. In this process, key points in the images are automatically extracted, described, and finally matched. The second step is photogrammetric triangulation based on bundle adjustment algorithm. Here, the matched key points, which have been obtained from image matching, along with GCPs are utilized to determine the interior and exterior orientation parameters for each image and 3D point locations of key points forming spare point clouds [17].

Data georeferencing can be performed either by direct or indirect methods. Direct georeferencing can be achieved using the camera position information of a GNSS, recorded by the onboard receiver during UAV flight. Although this method is faster and more economical, indirect georeferencing method can be applied using a set of GCPs that are distinctly identifiable in related images. To apply indirect georeferencing, some of the 18 ground reference points were used as GCPs and the remaining were utilized as check points (CPs) for assessment of positioning accuracy of generated point clouds. On the other hand, there are two methods to aligning images namely generic and reference aligning. In the generic aligning technique, all the images are chosen to be matched together through extracted key points. In the reference aligning method, the overlapping images are only selected based on the measured camera locations to be matched [18]. Experimentation using different setups adopting two percentages 60% and 80% of image overlap and available options of georeferencing and aligning were carried out. The results are analyzed to evaluate their impact on the positioning accuracy of generated point clouds. For each setup the accuracy is assessed throughout the computation of deviations at CPs between the reference GNSS data and UAV-derived data.

Also, in order to evaluate the impact of image resolution, and selected limits of key/tie points on the geometric accuracy of generated point cloud, another set of experiments were executed utilizing different setups in which different image resolutions, and different limits of key/tie points are considered.

It is worth mentioning that the system used for processing was Dell G3 with Intel Core i7-10750H CPU @ 2.60GHz processor, 16.0 GB installed ram, and 64-bit operating system.

5.RESULTS AND DISCUSSIONS

As explained in Section 4 above the first set of experiments was carried out considering the influence of image overlap, georeferencing technique and aligning approach on the positioning accuracy. Figure 4 illustrates the related scheme. It is worth mentioning that indirect georeferencing experiments were implemented using the more accurate aligning approach based on the results obtained from direct georeferencing experiments. The following subsections present the results of performed experimentation.

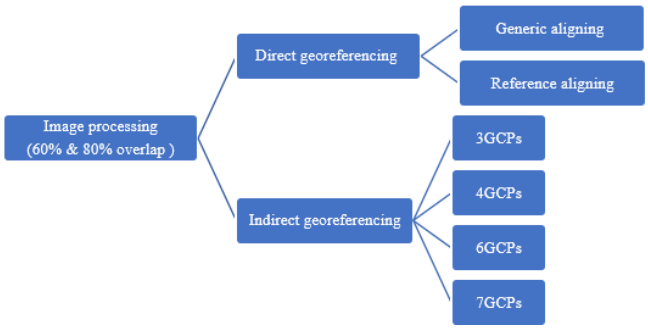

FIG 4. Data processing scheme considering image overlap percentage, georeferencing technique and aligning approach

5.1 Direct Georeferencing with 60% and 80% Image Overlap

Direct georeferencing does require using any GCPs. It was performed in this research with 60% and 80% image overlap based first on generic aligning and second on reference aligning as shown in the next two subsections. In this regard, all ground reference points are used as check points.

5.1.1 *Direct Georeferencing Based on Generic Aligning*

The alignment process of large sets of images can take a long time. Most of this time is consumed through matching of extracted features on the images. In the generic aligning, the overlapping pairs of images are selected by matching them using lower accuracy setting first. In this section, the geometric accuracy of UAV point clouds obtained by generic aligning was presented by statistical analysis of the differences among CPs coordinates derived from this method and their coordinates derived from static GNSS surveying. Results for 60% and 80% overlap are summarized in Table 1. It can be clearly observed that the total RMS of the differences has been improved by 40% when the overlap increased from 60% to 80%.

5.1.2 *Direct Georeferencing Based on Reference Aligning*

In the reference aligning, the overlapping pairs of photos are selected based on the measured camera locations. The geometric accuracy of UAV point clouds generated by reference aligning was presented by statistical analysis of the differences among CPs coordinates derived from this method and corresponding coordinates obtained by static GNSS surveying. Results for 60% and 80% overlap are summarized in Table 2. It can be drawn that at increasing the overlap from 60% to 80%, total RMS of differences has been improved by 29%.

TABLE 1. Statistics of coordinate differences of CPs in meters considering 60% and 80% overlap, direct georeferencing and generic aligning

Statistic	60% Overlap			80% Overlap		
	East	North	Elevation	East	North	Elevation
Min. difference	0.000	0.001	0.000	0.003	0.000	0.000
Max. difference	0.078	0.038	0.088	0.048	0.042	0.039
Mean of differences	0.028	0.019	0.033	0.021	0.015	0.015
RMS of differences	0.037	0.022	0.042	0.025	0.018	0.019
Total RMS of differences	0.060			0.036		

TABLE 2. Statistics of coordinate differences in meters of CPs considering 60% and 80% overlap, direct georeferencing and reference aligning

Statistic	60% Overlap			80% Overlap		
	East	North	Elevation	East	North	Elevation
Min. difference	0.003	0.000	0.001	0.001	0.004	0.000
Max. difference	0.053	0.033	0.067	0.041	0.035	0.047
Mean of differences	0.022	0.016	0.029	0.017	0.015	0.015
RMS of differences	0.028	0.019	0.035	0.020	0.018	0.021
Total RMS of differences	0.048			0.034		

TABLE 3. Statistics of absolute coordinate differences in meters of CPs considering indirect geo-referencing and reference aligning based on 3 GCPs

Statistic	60% Overlap			80% Overlap		
	East	North	Elevation	East	North	Elevation
Min. difference	0.003	0.000	0.035	0.000	0.001	0.001
Max. difference	0.070	0.045	0.194	0.041	0.041	0.102
Mean of differences	0.028	0.020	0.102	0.022	0.023	0.052
RMS of differences	0.032	0.024	0.113	0.024	0.027	0.059
Total RMS of differences	0.120			0.069		

5.2 Indirect Georeferencing with 60% and 80% Image Overlap

Indirect georeferencing using GCPs has been applied using reference aligning and different numbers of well distributed GCPs to investigate their impact on the accuracy of UAV photogrammetric solution. Here, all captured images were processed using four different cases of GCPs distribution. Numbers of GCPs used in the four cases are 3, 4, 6 and 7, respectively.

5.2.1 *Indirect georeferencing based on 3 GCPs*

This was the first case of indirect georeferencing applied, where points of numbers p211, p302 and p306 shown in Fig. 5 were used as control points.

The positioning accuracy of UAV point clouds generated by indirect georeferencing based on 3 GCPs was presented by statistical analysis of the differences among CPs coordinates derived from this method and corresponding coordinates obtained by static GNSS surveying. The results for 60% and 80% overlap are summarized in Table 3. The tabulated values indicated that the total RMS of differences improved by 42.5% when overlap percentage increased from 60% to 80%.

FIG 5. Distribution of GCPs of case no.

5.2.2 *Indirect georeferencing based on 4 GCPs*

In this case, points of numbers p211, p209, p307 and p306 shown in Fig. 6 were used as control points.

Table 4 illustrates the obtained coordinate differences. It can be observed that total RMS of differences was enhanced by increasing the number of GCPs to 4 points. In addition, it improved by 47% when the overlap increased from 60% to 80%.

FIG 6. Distributions of GCPs of case no.2

TABLE 4. Statistics of absolute coordinate differences in meters of CPs considering indirect geo-referencing and reference aligning based on 4 GCPs

Statistic	60% Overlap			80% Overlap		
	East	North	Elevation	East	North	Elevation
Min. difference	0.002	0.000	0.016	0.004	0.000	0.003
Max. difference	0.066	0.038	0.151	0.037	0.036	0.086
Mean of differences	0.016	0.015	0.085	0.017	0.016	0.038
RMS of differences	0.023	0.019	0.097	0.020	0.020	0.046
Total RMS of differences	0.102			0.054		

TABLE 5. Statistics of absolute coordinate differences in meters of CPs considering indirect geo-referencing and reference aligning based on 6 GCPs

Statistic	60% Overlap			80% Overlap		
	East	North	Elevation	East	North	Elevation
Min. difference	0.000	0.004	0.006	0.004	0.001	0.011
Max. difference	0.032	0.032	0.137	0.027	0.034	0.081
Mean of differences	0.016	0.016	0.060	0.016	0.016	0.039
RMS of differences	0.018	0.019	0.074	0.018	0.019	0.046
Total RMS of differences	0.078			0.053		

TABLE 6. Statistics of absolute coordinate differences in meters of CPs considering indirect geo-referencing and reference aligning based on 7 GCPs

Statistic	60% Overlap			80% Overlap		
	East	North	Elevation	East	North	Elevation
Min. difference	0.001	0.001	0.008	0.006	0.000	0.002
Max. difference	0.042	0.040	0.109	0.035	0.042	0.038
Mean of differences	0.017	0.015	0.035	0.018	0.017	0.021
RMS of differences	0.021	0.018	0.045	0.020	0.021	0.024
Total RMS of differences	0.053			0.038		

5.2.3 *Indirect georeferencing based on 6 GCPs*

This is the third case of indirect georeferencing. In this case, points of numbers p211, p209, p307, p306, p302 and p304 illustrated in Fig. 7 were used as control points.

Table 5 demonstrates the obtained coordinate differences. As occurred in the second case, the total RMS became better by increasing the number of GCPs to 5 points. Also, it improved by 32% when the overlap increased from 60% to 80%.

FIG7. Distributions of GCPs of case no.3

5.2.4 *Indirect geo-referencing based on 7 GCPs*

In this fourth case, points of numbers p211, p209, p307, p306, p302, p304 and p205 shown in Fig. 8 were used as control points.

The resulted coordinate differences of this case are demonstrated in Table 6. It can be noted that the accuracy was enhanced by increasing the number of GCPs to 7 points. Besides, it improved by 28% when the overlap increased from 60% to 80%.

FIG 8. Distributions of GCPs of case no.4

5.3 Impact of Image Resolution, and limits of Key/Tie points

The parameters used through the aligning procedure by the software include image resolution and limits of key/tie points. While at high resolution setting the software works with the images of original size, the medium setting causes image downscaling by factor of 4. At low resolution, images are downscaled by factor of 16 [18]. Key point limit indicates upper limit of feature points on every image to be taken into account during current processing stage. Tie point limit indicates upper limit of matching points for each image. In this section three cases of image resolution were tested and analyzed to evaluate the impact on positioning accuracy, processing time and number of points of generated point clouds by UAV imagery. For each case, two combinations of key/tie points limits were tried as shown in Fig. 9. The implemented tests adopted 80% overlap, direct georeferencing and reference aligning.

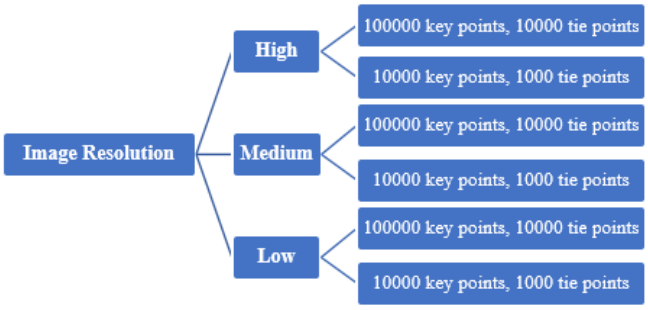

FIG 9. Data processing scheme considering image resolution, key points and tie points

5.3.1 *High image resolution*

This is the first case where high image resolution is considered; along with the two combinations of key/tie points limits. Table 7 summaries the obtained results. It can be clearly observed that increasing the number of key/tie points has enhanced the positioning accuracy by 43%. On the other hand, density of point cloud also increased immensely.

5.3.2 *Medium image resolution*

The second case considered is the medium image resolution, with the two combinations of key/tie points limits used above. Table 8 shows that obtained positioning accuracy, matching time and density of point cloud decreased compared with the first case.

TABLE 7. Statistics of absolute coordinate differences in meters of CPs, matching time and size of point cloud considering high image resolution and using two different combinations of key/tie points limits

Statistic	100000 key pts. / 10000 tie pts.			10000 key pts. / 1000 tie pts.		
	East	North	Elevation	East	North	Elevation
Min. difference	0.001	0.004	0.000	0.001	0.005	0.003
Max. difference	0.041	0.035	0.047	0.030	0.065	0.082
Mean of differences	0.017	0.015	0.015	0.015	0.029	0.042
RMS of differences	0.020	0.018	0.021	0.018	0.033	0.047
Total RMS of differences	0.034			0.060		
Matching Time	19 min16 sec			3 min 21 sec		
Number of points	165281			13484		

TABLE 8. Statistics of absolute coordinate differences in meters of CPs, matching time and size of point cloud considering medium image resolution and using two different combinations of key/tie points limits

Statistic	100000 key pts. / 10000 tie pts.			10000 key pts. / 1000 tie pts.		
	East	North	Elevation	East	North	Elevation
Min. difference	0.001	0.003	0.002	0.005	0.001	0.001
Max. difference	0.060	0.083	0.094	0.046	0.074	0.130
Mean of differences	0.022	0.038	0.026	0.020	0.031	0.028
RMS of differences	0.029	0.044	0.035	0.023	0.037	0.040
Total RMS of differences	0.062			0.059		
Matching Time	3 min 21 sec			2 min 39 sec		
Number of points	87731			11470		

TABLE 9. Statistics of absolute coordinate differences in meters of CPs, matching time and size of point cloud considering low image resolution and using two different combinations of key/tie points limits

Statistic	100000 key pts. / 10000 tie pts.			10000 key pts. / 1000 tie pts.		
	East	North	Elevation	East	North	Elevation
Min. difference	0.000	0.001	0.008	0.001	0.011	0.021
Max. difference	0.155	0.099	0.358	0.111	0.183	0.448
Mean of differences	0.052	0.039	0.115	0.054	0.067	0.149
RMS of differences	0.065	0.049	0.137	0.064	0.081	0.174
Total RMS of differences	0.160			0.202		
Matching Time	54 sec			56 sec		
Number of points	24042			12839		

TABLE 10. Statistics of absolute coordinate differences in meters of CPs and processing time for resulted orthomosaic in case of 80% overlap and direct georeferencing technique

Statistic	Easting	Northing
Min. difference	0.001	0.003
Max. difference	0.041	0.038
Mean of differences	0.017	0.016
RMS of differences	0.020	0.019
Total RMS of differences	0.028	
Processing time	6 hours 49 minutes 29 seconds	

TABLE 11. Statistics of absolute coordinate differences in meters of CPs and processing time for resulted orthomosaic in case of 80% overlap and indirect georeferencing technique

Statistic	Easting	Northing
Min. difference	0.005	0.001
Max. difference	0.035	0.055
Mean of differences	0.018	0.021
RMS of differences	0.009	0.017
Total RMS of differences	0.019	
Processing time	6 hours one minutes 5 seconds	

5.3.3 *Low image resolution*

In this case low image resolution has been considered. Low image resolution resulted in lower positioning accuracy as well as lower matching time and density of point compared with the first two cases, as exhibited in Table 9.

5.4 Accuracy Assessment of Generated Orthomosaic

In this section, the geometric accuracy of orthomosaic generated from UAV point cloud was assessed. This was done through a statistical analysis of the differences among CPs coordinates derived from the generated orthoimage and their coordinates derived from static GNSS surveying. Two setups are used for this purpose. The first setup used 80% overlap with direct

georeferencing and reference aligning. Table 10 shows the statistics of obtained coordinate differences as well as processing time spent in generating the orthoimage.

The second setup used 80% overlap with indirect georeferencing and reference aligning (case no. 4, section 5.2.4) for generating the orthmosaic. Table 11 illustrates the statistics of obtained coordinate differences as well as processing time spent in generating the orthoimage. The resulted total RMS in this case is 0.019 m, which is better compared with total RMS obtained in the first case.

6.CONCLUSIONS

For UAV photogrammetry, the positioning accuracy of the generated point cloud is affected by many variables such as percentage of overlap, georeferencing technique, configuration of GCPs, image resolution, as well as matching variables. Higher degree of overlap improved positioning accuracy of the generated point cloud. Direct georeferencing technique with no GCPS yielded good positioning accuracy. Indirect georeferencing technique and increasing the number of GCPs achieved equivalent positioning accuracy. Higher image resolution resulted in higher positioning accuracy. Decreasing the number of key/tie points led to lower positioning accuracy and less processing time. Generated orthomosaic for the test area has achieved high accuracy considering each of the two georeferencing techniques. As future work, the obtained point cloud and orthomosaic can be fused and evaluated for 3D city model generation

REFERENCES

[1] I. Colomina and P. Molina, "Unmanned aerial systems for photogrammetry and remote sensing: A review," ISPRS Journal of Photogrammetry and Remote Sensing, vol. 92. 2014.

[2] F. C. Nogueira, L. Roberto, T. S. Körting, and E. H. Shiguemori, "Accuracy analysis of orthomosaic and DSM produced from sensor aboard UAV," XVIII Simpósio Brasileiro de Sensoriamento Remoto SBSR, 2017.

[3] O. Küng et al., "The Accuracy Of Automatic Photogrammetric Techniques On Ultra-Light Uav Imagery," The International Archives of the Photogrammetry, Remote Sensing and Spatial Information Sciences, vol. XXXVIII-1/C22, 2012.

[4] S. Rhee and T. Kim, "Automated DSM extraction from UAV images and performance analysis," in International Archives of the Photogrammetry, Remote Sensing and Spatial Information Sciences - ISPRS Archives, 2015.

[5] M. Gerke, "Developments in UAV-Photogrammetry," Journal of Digital Landscape Architecture, no. 3, 2018.

[6] E. Sanz-Ablanedo, J. H. Chandler, J. R. Rodríguez-Pérez, and C. Ordóñez, "Accuracy of Unmanned Aerial Vehicle (UAV) and SfM photogrammetry survey as a function of the number and location of ground control points used," Remote Sens (Basel), vol. 10, no. 10, 2018.

[7] G. Pessoa, A. Caceres Carrilho, G. Takahashi Miyoshi, A. Amorim, and M. Galo, "Assessment of UAV-based digital surface model and the effects of quantity and distribution of ground control points," Int J Remote Sens, vol. 42, no. 1, 2021.

[8] F. Agüera-Vega, F. Carvajal-Ramírez, and P. Martínez-Carricondo, "Accuracy of Digital Surface Models and Orthophotos Derived from Unmanned Aerial Vehicle Photogrammetry," Journal of Surveying Engineering, vol. 143, no. 2, 2017.

[9] I. Elkhrachy, "Accuracy Assessment of Low-Cost Unmanned Aerial Vehicle (UAV) Photogrammetry," Alexandria Engineering Journal, vol. 60, no. 6, 2021.

[10] D. Domingo, H. Ørka, E. Næsset, D. Kachamba, and T. Gobakken, "Effects of UAV Image Resolution, Camera Type, and Image Overlap on Accuracy of Biomass Predictions in a Tropical Woodland," Remote Sensing (Basel), vol. 11, no. 8, 2019.

[11] N. Snavely, "Scene reconstruction and visualization from internet photo collections: A survey," IPSJ Transactions on Computer Vision and Applications, vol. 3, 2011.

[12] M. Spetsakis and J. Y. Aloimonos, "A multi-frame approach to visual motion perception," Int J Comput Vis, vol. 6, no. 3, 1991.

[13] B. Boufama, R. Mohr, and F. Veillon, "Euclidean constraints for uncalibrated reconstruction," in 1993 IEEE 4th International Conference on Computer Vision, 1993.

[14] C. Harris and M. Stephens, "A Combined Corner and Edge Detector," 2013.

[15] M. J. Westoby, J. Brasington, N. F. Glasser, M. J. Hambrey, and J. M. Reynolds, "Structure-from-Motion photogrammetry: A low-cost, effective tool for geoscience applications," Geomorphology, vol. 179, 2012.

[16] A. Lucieer, S. Robinson, D. Turner, S. Harwin, and J. Kelcey, "Using A Micro-Uav For Ultra-High Resolution Multi-Sensor Observations Of Antarctic Moss Beds," The International Archives of the Photogrammetry, Remote Sensing and Spatial Information Sciences, vol. XXXIX-B1, 2012.

[17] M. Cramer, D. Stallmann, and N. Haala, "Direct georeferencing using gps/inertial exterior orientations for photogrammetric applications," International Archives of Photogrammetry and Remote Sensing, vol. 33, no. B3, 2000.

[18] Agisoft, "Agisoft Metashape User Manual," Agisoft Metashape, no. September, 2020.